Supplementary Information

Unravelling Quantum Dot–Molecule Interactions for π-Conjugated Ligands: Insights into Binding and Anchoring Group Effects

Yinon Deree, Adar Levi, Xiang Li, Ori Gidron* and Uri Banin*

Institute of Chemistry and the Center for Nanoscience and Nanotechnology, The Hebrew University.

Contents

Chemicals

Oleylamine (OAm, 70%), oleic acid (OA, 99%), 1-octadecene (ODE, 90%), cadmium oxide (CdO, ≥99.99%), selenium (Se, 99.99%), trioctylphosphine oxide (TOPO, 99%), and 9-anthracenemethanol were purchased from Sigma Aldrich. Trioctylphosphine (TOP, 97%) was purchased from Strem Chemicals. Octadecylphosphonic acid (ODPA, >99%) was purchased from PCI. 9-Anthracenecarboxylic acid, 9,10-Bis(chloromethyl)anthracene was purchased from BLD. All the reagents were used as received without further purification. AT was synthesized according to reported procedure[1] and ADT was synthesized according to reported procedure[2] and its identity was confirmed by ^{1}H NMR spectroscopy, in agreement with previously reported spectral data.

Characterization

Flash chromatography (FC) was performed using CombiFlash SiO_2 columns. 1H spectra were recorded in solution on a Bruker-AVIII 400 MHz and 500 MHz spectrometers using tetramethylsilane (TMS) as the external standard. The spectra were recorded using chloroform-d as the solvent. Chemical shifts are expressed in δ units. UV-vis absorption spectra were recorded with an Agilent Cary-5000 spectrophotometer. The spectra were measured using a quartz cuvette (1 cm) at 25 °C. Steady-state fluorescence measurements were performed on a HORIBA JOBIN YVON Fluoromax-4 spectrofluorometer The lifetimes of the excited species were measured using an NL-C2 Pulsed Diode Controller NanoLED light source with time-correlated single proton counting (TSCPC) Controller DeltaHub (HORIBA), referenced against colloidal Ludox solution (50 wt. % solution in water) obtained from Aldrich. Transmission electron microscopy (TEM) was performed using a Tecnai G² Spirit Twin T12 microscope (Thermo Fisher Scientific) operated at 120 kV. Particle size analysis was conducted by measuring individual particles from TEM images.

H-NMR of AT and ADT

ADT

^{1}H NMR (400 MHz, $CDCl_3$) δ 8.37 – 8.28 (m, 4H), 7.65 – 7.56 (m, 4H), 4.73 (d, *J* = 6.8 Hz, 4H), 1.98 (t, *J* = 6.8 Hz, 2H).

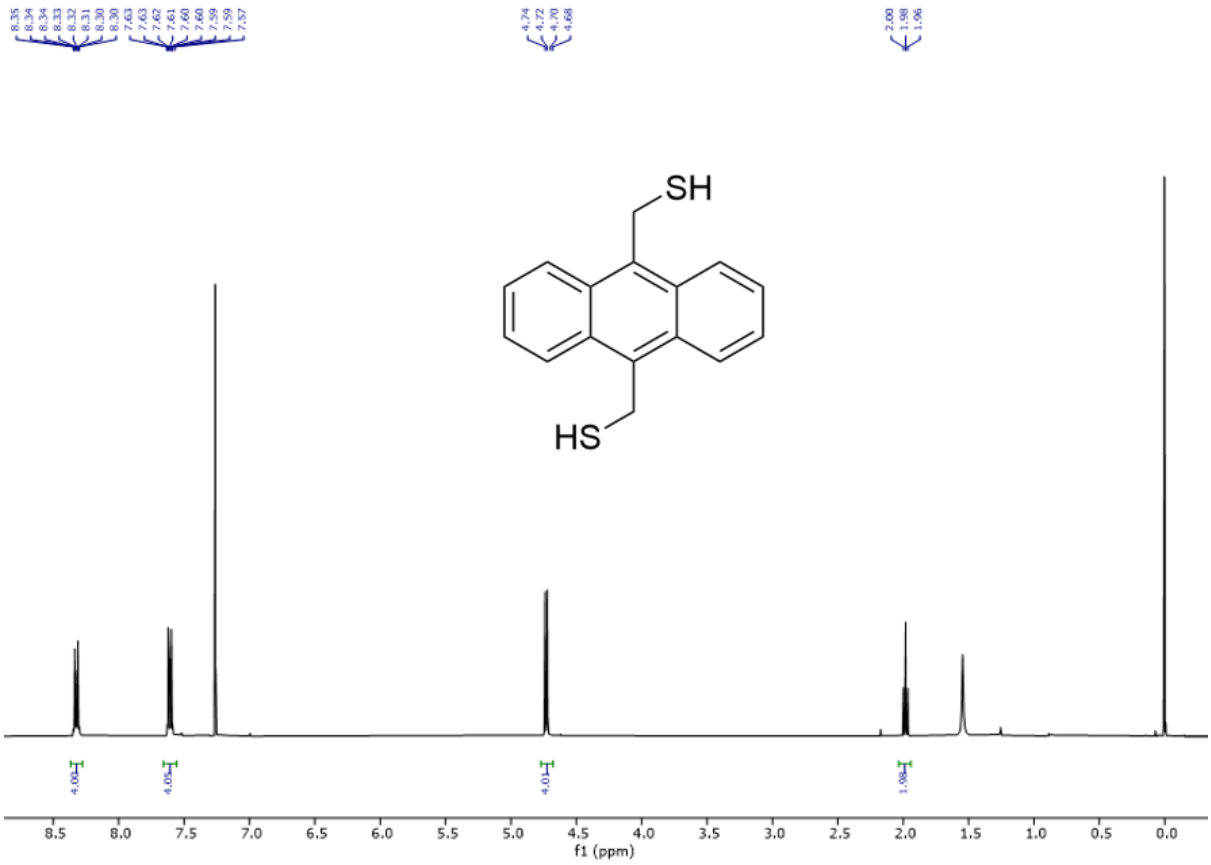

AT

^{1}H NMR (400 MHz, $CDCl_3$) δ 8.41 (s, 1H), 8.26 (dt, *J* = 8.9, 1.0 Hz, 2H), 8.03 (ddt, *J* = 8.3, 1.2, 0.6 Hz, 2H), 7.58 (ddd, *J* = 8.9, 6.5, 1.4 Hz, 2H), 7.53 – 7.45 (m, 2H), 4.74 (s, 2H), 1.97 (br, 1H).

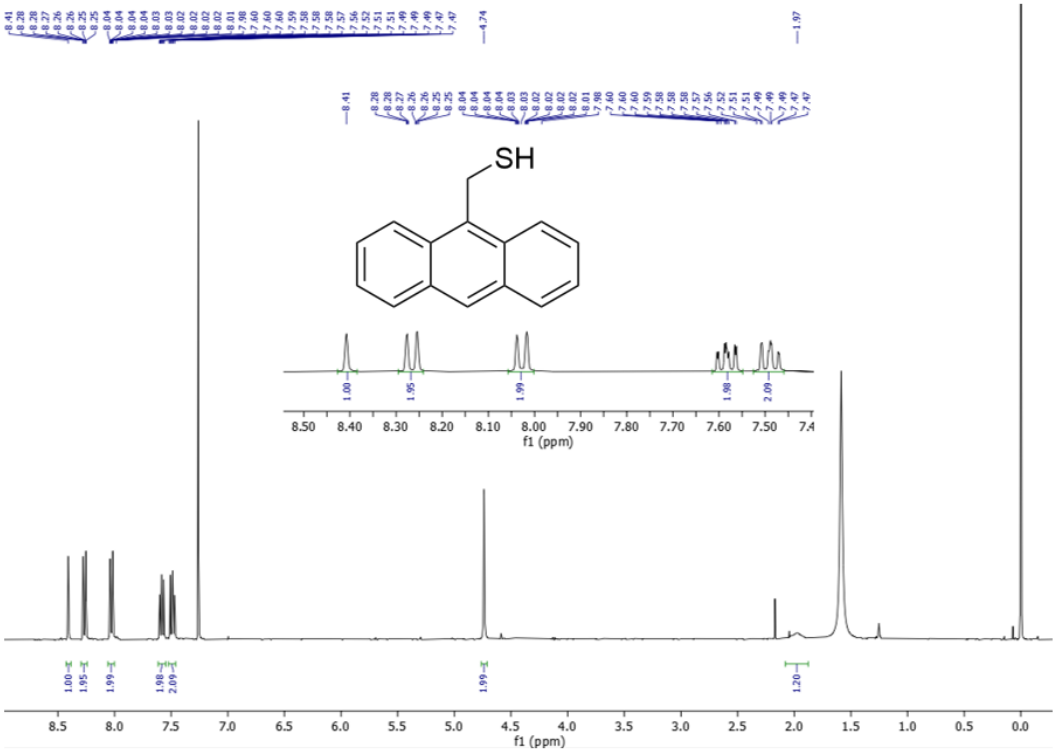

CdSe QDs Synthesis

Stock solutions

In a 150 mL three-neck flask, 24 mmol CdO and 60 mL OA were degassed under vacuum at 120°C for 1 hour. The temperature was increased to 200°C under argon flow until the solution turned clear. Then, the mixture was cooled to 70°C, 60 mL ODE was added, and the solution was degassed again under vacuum for 1 hour to produce a 0.2 M Cd-oleate solution.

Se-ODE suspension (0.1 M): 0.6 mmol of Se powder were mixed with 6 ml of ODE and sonicated for at least 1 hour prior to their use in the synthesis.

CdSe nanocrystal (NC) synthesis

CdSe NC syntheses are based on well-established procedures for both zinc blende and wurtzite crystal structures.

Oleic acid-coated Zinc Blende NCs:[3]

In a 100 mL three-neck flask, 4 mL of 0.2 M Cd-oleate and 13 mL of ODE were degassed under vacuum at 100°C for 1 hour. The temperature was then increased to 240°C under argon flow, and 4 mL of 0.1 M Se-ODE suspension was quickly injected. The nanocrystals reached the desired size after 5 minutes of growth. The resulting NCs were washed using ethanol and dispersed in toluene.

Phosphonic acid-coated Wurtzite NC:[4]

60 mg CdO, 280 mg ODPA, and 3 g TOPO were added to a 50 mL flask and degassed at 150°C under vacuum for 1 hour. Under argon, the mixture was heated to 320°C until a colorless solution formed. After adding 1.0 mL TOP, the temperature was raised to 350°C, followed by swift injection of Se/TOP solution (60 mg Se in 0.5 mL TOP). The reaction proceeded at 350°C until completion, then was cooled by removing the heating mantle. NCs were precipitated with acetone and dispersed in 3 mL hexane for storage.

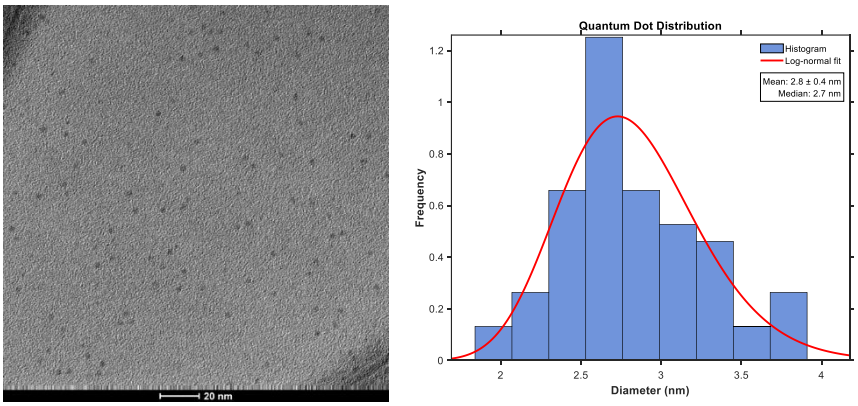

Figure Sa. (left panel) TEM image and (right panel) size distribution histogram of synthesized CdSe QDs showing narrow size distribution with mean diameter of 2.8 ± 0.4 nm. Scale bar: 20 nm.

Ligand exchange and photophysical properties

After preparing the QDs, we simply added ligands to a cuvette with the QDs.

Detailed explanation:

A ligand solution was prepared at a known concentration (~1M). Similarly, QDs were dispersed in a known volume (3 mL) and concentration(3Mm-4mM), as determined from the optical density (OD) shown in Figures S11–S14. The QD concentration was calculated using the known extinction coefficient at the first excitonic absorption peak. Fixed volumes of 5 µL of the ligand solution were sequentially added to the QD dispersion. Given that the QD solution volume exceeds the added ligand volumes by approximately three orders of magnitude, any observed photoluminescence quenching can be attributed to ligand–QD interactions rather than to dilution or changes in QD concentration.

It is critical to clean the QDs stock solution from free OA as they can affect the binding of the ligands (Figure S2 and S9), specifically the ACA as it has relative weak binding group. The thiol ligand bound easily also in the case of the TOP/TOPO/ODPA ligands.

Name	$\varepsilon(cm^{-1}M^{-1})$
QD-OA[5]	$1.4{\cdot}10^5$
ACA	7500
AT	8500
ADT	7400

Table S1. Molar absorption coefficients of the ligands and OA-QD, with ligand values corresponding to the lowest-energy vibronic peak maximum.

QD lifetime were fitted to tri exponential decay:

$$f(t) = A_1 e^{-\frac{t}{\tau_1}} + A_2 e^{-\frac{t}{\tau_2}} + A_3 e^{-\frac{t}{\tau_3}}$$

A_1	0.11
A_2	$5.11 \cdot 10^{-2}$
A_3	$8.26 \cdot 10^{-3}$
τ_1	$2.6ns$
τ_2	$19.5ns$
τ_3	$91.6ns$

The average life time:

$$< \tau >= \frac{A_1\tau_1 + A_2\tau_2 + A_3\tau_3}{A_1 + A_2 + A_3} = 12.1ns$$

Equilibrium Model

Reaction: $ACA{+}OA{-}QD \rightleftharpoons ACA{-}QD + OA$

Equilibrium constant:

$$(1)\ \mathrm{K_{eq}} = \frac{[\mathrm{QD{-}ACA}][\mathrm{OA}]}{[\mathrm{ACA}][\mathrm{QD{-}OA}]}$$

Where [ACA] is free ACA concentration, [QD-OA] is the bound OA concentration, [QD-ACA] is the bound ACA concentration and [OA] is free OA concentration.

If there is no free OA present before ACA was added then [QD-ACA] = [OA] meaning:

$$(2)\ \mathrm{K_{eq}} = \frac{[\mathrm{QD{-}ACA}]^2}{[\mathrm{ACA}][\mathrm{QD{-}OA}]}$$

and by applying the law of conservation of mass along with the initial condition:

$$(3)\ \mathrm{K_{eq}} = \frac{[QD-ACA]^2}{([ACA]_0-[QD-ACA])([QD-OA]_0-[QD-ACA])}$$

Where $[ACA]_0$ is the ACA add to the solution and $[QD\text{-}OA]_0$ is the bound OA concentration before any ACA added.

in addition:

$$(4)\ [QD\text{-}OA]_0 = [QD]_0 \cdot \#_{cd}$$

Where $[QD]_0$ is the QD concentration and $\#_{cd}$ is the number of Cd sites on the surface of the QD.

$[QD]_0$ is known from the absorption and the $\#_{cd}$ can be estimated by a simple spherical model or by simulated atomistic model for zinc blend CdSe[6]. Both calculations give results that are approximately equal to 100 Cd sites for the size of QDs used in our study.

$$(5)\ \mathrm{K_{eq}} = \frac{[QD-ACA]^2}{([ACA]_0-[QD-ACA])(100[QD]_0-[QD-ACA])}$$

We can isolate [QD-ACA] and right it as function of $[ACA]_0$:

$$(6)\ [QD-ACA] = \frac{-K_{eq}([ACA]_0+100[QD]_0)\left(\left(K_{eq}([ACA]_0+100[QD]_0\right)^2+4\left(1-K_{eq}\right)K_{eq}100[QD]_0[ACA]_0\right)^{0.5}}{2(1-K_{eq})}$$

Using all the above we can plot [QD-ACA] vs $[ACA]_0$:

https://www.desmos.com/calculator/h7ym5tjvql

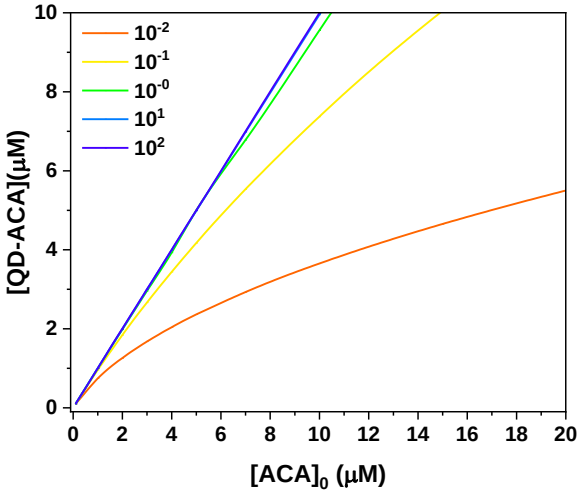

Figure S1. [QD-ACA] vs $[ACA]_0$ for different values of the equilibrium constant (K_{eq}) represented as 10^x.

The region of a linear relationship (y=x) means that [QD-ACA] = $[ACA]_0$, where all added ACA ligands are bound to QD. linearity holds when $[ACA]_0 << [OA\text{-}QD]_0$, or when K_{eq} is large.

If free OA ligands are present than the equilibrium equation has the form:

$$K_{eq} = \frac{[QD-ACA]([OA]_0+[QD-ACA])}{([ACA]_0-[QD-ACA])(100[QD]_0-[QD-ACA])}$$

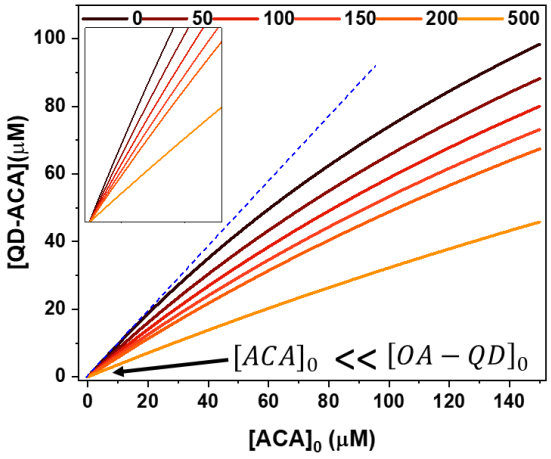

Figure S2. [QD-ACA] vs $[ACA]_0$, the numbers are the initial free OA number concentrations in the solution. The blue linear line is the graph y=x.

in the absence of free OA and under the condition $[ACA]_0 << [OA\text{-}QD]_0$ the graph exhibits a linear relationship with a slope of 1 (i.e, y=x). This indicates that, in this limit, all added ACA molecules are bound to the QDs. Furthermore, when free OA ligands

are present, the graph remains linear in the same limit $[ACA]_0 << [OA\text{-}QD]_0$ but deviates from a slope equal to 1. This deviation suggests that in the presence of free OA, the addition of ACA results in two distinct populations: free ACA and QD-bound ACA even at low ACA concentration. Therefore, it is critical to clean excess OA ligands before ACA addition.

QDs SV model and experiment

In order to develop an expression for the functional form of SV y axes ($\frac{I_0}{I(x)}$, I_0 – PL intensity with no ligands, I(x) - PL intensity with x average bound ligands) we will assume a Poisson distribution of the ligands bound to the QDs and that the quantum yield (QY) of one QD with n ligands has the form of:

(1) $\phi(n) = \frac{k_r}{k_r + k_{nr} + nk_q}$

Where $\phi(n)$ is the quantum yield of QDs with n bound ligands, k_r is the average radiative rate constant, k_{nr} is the average non-radiative rate constant and k_q is the quenching rate constant of single molecule bound to the QD.

In addition, the probability of QD to be with n ligands according to the Poisson distribution:

(2) $p(n) = \frac{x^n}{n!} e^{-x}$

Where $p(n)$ is probability of QD to be with n ligands and x is the average number of bound ligands.

Combining equations 1 and 2 will give the average quantum yield as function of average number of bound ligands:

(3) $\bar{\phi}(x) = \sum_{n=1}^{\infty} p(n)\,\phi(n) = \sum_{n=1}^{\infty} \frac{x^n}{n!} e^{-x} \frac{k_r}{k_r + k_{nr} + nk_q}$

Since PL intensity (I(x)) is linear with quantum yield the ratio of $I_0/I(x)$ is equal to the ratio $\phi_0/\bar{\phi}(x)$:

(4) $$\frac{\phi_0}{\bar{\phi}(x)} = \frac{I_0}{I(x)} = \frac{\frac{k_r}{k_r + k_{nr}}}{\sum_{n=1}^{\infty} \frac{x^n}{n!} e^{-x} \frac{k_r}{k_r + k_{nr} + nk_q}}$$

(5) $$\frac{\phi_0}{\bar{\phi}(x)} = \frac{I_0}{I(x)} = \frac{\frac{k_r}{k_r + k_{nr}}}{\sum_{n=1}^{\infty} \frac{x^n}{n!} e^{-x} \frac{k_r}{k_r + k_{nr} + nk_q}} = \frac{\frac{1}{k_r + k_{nr}}}{\sum_{n=1}^{\infty} \frac{x^n}{n!} e^{-x} \frac{1}{k_r + k_{nr} + nk_q}} = \frac{\frac{k_q}{k_r + k_{nr}}}{\sum_{n=1}^{\infty} \frac{x^n}{n!} e^{-x} \frac{1}{\frac{k_r + k_{nr}}{k_q} + n}}$$

We will define parameter b in the following way:

(6) $b = \frac{k_r + k_{nr}}{k_q}$

Therefore, equation 1 one can be written as follows:

(7) $\frac{I_0}{I(x)} = \frac{b^{-1}}{\sum_{n=1}^{\infty} \frac{x^n}{n!} e^{-x} \frac{1}{b+n}}$

Equation 7 has Several interesting limits:

(8) $\lim_{b\to 0} \frac{I_0}{I(x)} = e^x$

(9) $\lim_{b\to \infty} \frac{I_0}{I(x)} = 1 + \frac{x}{b}$

(10) $\lim_{b\to 1} \frac{I_0}{I(x)} = \frac{xb^{-1}}{(1-e^{-x})e^{1-b}}$ and if also x is large the term equal to $\lim_{b\to 1} \frac{I_0}{I(x)} = x$

And as mentioned in the paper, if x is large the function is approaching linearity.

- Two approaches to understanding why added ligands exhibit a Poisson distribution across the QDs:

The assumption in both approaches is that adsorption is a random process and that all adsorption sites are equivalent. This holds true only when ligand coverage is low, since at high coverage, interactions between neighboring ligands occur, leading to cooperative or anti-cooperative effects.

1) Statistical approach:

Suppose we have m ligands and n QDs. When ligands are added to a solution containing n QDs, each ligand randomly adsorbs onto one of the QDs. That is, each ligand has a probability of 1/n to adsorb onto a given QD. If we focus on a specific QD in the solution, we can consider each ligand as a Bernoulli trial (success = adsorption onto this nanocrystal, failure = adsorption onto another one). Therefore, with m ligands in the solution, we effectively have m independent Bernoulli trials. Thus, the number of ligands adsorbed onto a given QD follows a binomial distribution. The probability that a QD has exactly k ligands is given by:

$$p(k) = \binom{m}{k} \left(\frac{1}{n}\right)^k \left(1 - \frac{1}{n}\right)^{m-k}$$

Now, consider the limit as n → ∞ and m → ∞, while keeping the ratio m/n constant and equal to λ. Physically, this limit reflects the experimental condition where m and n are on the order of Avogadro number. From this, we get that λ/m = 1/n, and we can rewrite the binomial probability as follows:

$$p(k) = \binom{m}{k} \left(\frac{\lambda}{m}\right)^k \left(1 - \frac{\lambda}{m}\right)^{m-k}$$

And we now write explicitly the full term $\binom{m}{k}$:

$$p(k) = \frac{m \cdot (m-1) \cdots (m-k-1)}{k!} \left(\frac{\lambda}{m}\right)^k \left(1 - \frac{\lambda}{m}\right)^{m-k}$$

$$p(k) = \frac{m \cdot (m-1) \cdots (m-k-1)}{k!} \cdot \frac{\lambda^k}{m^k} \left(1 - \frac{\lambda}{m}\right)^{m-k}$$

And we switch the order of the terms m^k-*ı* k!

$$p(k) = \frac{m \cdot (m-1) \cdots (m-k-1)}{m^k} \cdot \frac{\lambda^k}{k!} \left(1 - \frac{\lambda}{m}\right)^{m-k}$$

Let us now explicitly write the left-hand term

$$p(k) = \frac{m}{m} \cdot \frac{(m-1)}{m} \cdots \frac{(m-k-1)}{m} \cdot \frac{\lambda^k}{k!} \left(1 - \frac{\lambda}{m}\right)^{m-k}$$

And we split the rightmost term

$$p(k) = \frac{m}{m} \cdot \frac{(m-1)}{m} \cdots \frac{(m-k-1)}{m} \cdot \frac{\lambda^k}{k!} \left(1 - \frac{\lambda}{m}\right)^{m} \left(1 - \frac{\lambda}{m}\right)^{-k}$$

And we take the limit as m approaches infinity:

$$\lim_{m\to\infty} p(k) = \lim_{m\to\infty} \left(\frac{m}{m} \cdot \frac{(m-1)}{m} \cdots \frac{(m-k-1)}{m} \cdot \frac{\lambda^k}{k!} \left(1 - \frac{\lambda}{m}\right)^{m} \left(1 - \frac{\lambda}{m}\right)^{-k} \right)$$

The limit of a product is the product of the limits:

$$\lim_{m\to\infty} p(k) = \lim_{m\to\infty} \frac{m}{m} \cdot \lim_{m\to\infty} \frac{(m-1)}{m} \cdots \lim_{m\to\infty} \frac{(m-k-1)}{m} \cdot \lim_{m\to\infty} \frac{\lambda^k}{k!} \cdot \lim_{m\to\infty} \left(1 - \frac{\lambda}{m}\right)^{m} \cdot \lim_{m\to\infty} \left(1 - \frac{\lambda}{m}\right)^{-k}$$

All the limits from $\frac{m}{m}$ up to $\frac{(m-k-1)}{m}$ approach 1.

The limit $\lim_{m\to\infty} \frac{\lambda^k}{k!}$ is simply equal to $\lambda\frac{\lambda^k}{k!}$.

The limit $\lim_{m\to\infty} \left(1 - \frac{\lambda}{m}\right)^{m}$ is known and equals $e^{-\lambda}$

The limit $\lim_{m\to\infty} \left(1 - \frac{\lambda}{m}\right)^{-k}$ also equals 1.

Therefore:

$$\lim_{m\to\infty} p(k) = \frac{\lambda^k}{k!} e^{-\lambda}$$

2) Maximum entropy approach:

We seek the macrostate with the highest weight for m ligands distributed over n nanocrystals. The macrostate with the highest weight provides a good description of the system since m and n are large (maximum term approximation), The number of microstates corresponding to a macrostate with m ligands distributed over n identical nanocrystals is:"

$$\mathrm{W} = \frac{m!}{n_0!\, n_1! \cdots} = \frac{m!}{\prod_k n_k}$$

Let n_k be the number of nanocrystals with k ligands. Since the ligands are identical and there are k ligands on each nanocrystal, we must divide by $k!$ for each nanocrystal with k ligands. Therefore, the total number of microstates W is:

$$\mathrm{W} = \frac{m!}{\prod_k n_k (k!)^{n_k}}$$

The constraints are:

$$n = \sum_k n_k$$

$$m = \sum_k n_k k$$

We define the Lagrangian (to find the maximum of ln(W) subject to the constraints):

$$\mathrm{L} = \ln(W) - \alpha(\sum_k n_k - n) - \beta(\sum_k n_k k - m)$$

Let us expand W:

$$\mathrm{L} = \ln(m!) - \sum_k \ln(n_k!) - \sum_k n_k \ln(k!) - \alpha(\sum_k n_k - n) - \beta(\sum_k n_k k - m)$$

And we use Stirling approximation:

$$\mathrm{L} = \ln(m!) - \sum_k n_k \ln(n_k) - n_k - \sum_k n_k \ln(k!) - \alpha(\sum_k n_k - n) - \beta(\sum_k n_k k - m)$$

And we take the derivative with respect to n_k:

$$\frac{d\mathrm{L}}{dn_k} = -\ln(n_k) - \ln(k!) - \alpha - \beta k$$

The condition we obtained is:

$$\ln(n_k) = -\ln(k!) - \alpha - \beta k$$

Or in exponential form:

$$n_k = \frac{e^{-\alpha} e^{-\beta k}}{k!}$$

We use the first condition to solve for alpha:

$$\mathrm{n} = \sum_{\mathrm{k}} \mathrm{n_k}$$

$$n = \sum_k \frac{e^{-\alpha} e^{-\beta k}}{k!} = \sum_k \frac{e^{-\alpha} e^{-\beta k}}{k!} = e^{-\alpha} \sum_k \frac{e^{-\beta k}}{k!} = e^{-\alpha} \sum_k \frac{\left(e^{-\beta}\right)^k}{k!} = e^{-\alpha} e^{e^{-\beta}}$$

Therefore:

$$e^{-\alpha} = n e^{-e^{-\beta}}$$

Additionally, we use the second condition to solve for beta:

$$m = \sum_k n_k k$$

$$m = \sum_{k=0} n_k k = \sum_{k=0} \frac{e^{-\alpha} e^{-\beta k}}{k!} k = e^{-\alpha} \sum_{k=0} \frac{e^{-\beta k}}{k!} k = e^{-\alpha} \sum_{k=1} \frac{e^{-\beta k}}{k!} k = e^{-\alpha} \sum_{k=1} \frac{e^{-\beta k}}{(k-1)!}$$

We perform the variable substitution s=k-1:

$$m = e^{-\alpha} \sum_{k=1} \frac{e^{-\beta k}}{(k-1)!} = e^{-\alpha} \sum_{s=0} \frac{e^{-\beta(s+1)}}{s!} = e^{-\alpha} e^{-\beta} \sum_{s=0} \frac{\left(e^{-\beta}\right)^s}{s!} = e^{-\alpha} e^{-\beta} e^{e^{-\beta}}$$

And we substitute:

$$e^{-\alpha} = n e^{-e^{-\beta}}$$

$$m = e^{-\alpha} e^{-\beta} e^{e^{-\beta}} = n e^{-e^{-\beta}} e^{-\beta} e^{e^{-\beta}} = n e^{-\beta}$$

Therefore*:*

$$e^{-\beta} = \frac{m}{n}$$

As a reminder, $\frac{m}{n}$ is the average and is denoted by the letter λ.

Also: $e^{-\alpha} = n e^{-e^{-\beta}} = n e^{-\frac{m}{n}} = n e^{-\lambda}$.

As previously derived, we obtained:

$$n_k = \frac{e^{-\alpha} e^{-\beta k}}{k!}$$

And after substitution, we get:

$$n_k = \frac{n e^{-\lambda} \lambda^k}{k!}$$

And we divide by n:

$$\frac{n_k}{n} = p(k) = \frac{e^{-\lambda} \lambda^k}{k!}$$

We have again obtained a Poisson distribution from different considerations.

- For completeness, we include below the Desmos link showing the fit to the Poisson-based model, along with the corresponding linear Stern–Volmer fit plotted against the average number of ligands per QD.

ACA: https://www.desmos.com/calculator/rtmjkgeedz

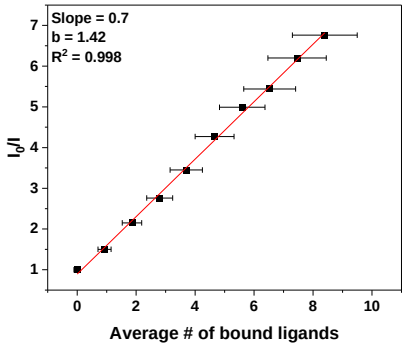

Figure Sb. SV experiment with ACA ligand.

PT: https://www.desmos.com/calculator/adaz4eewnk

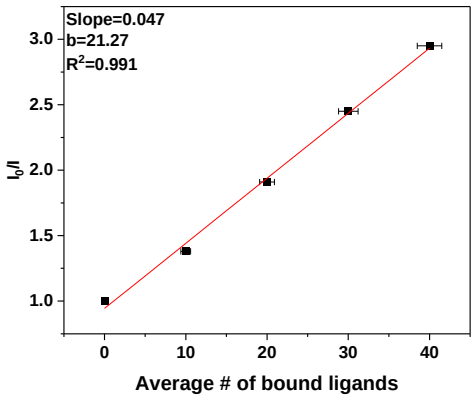

Figure Sc. SV experiment with PT ligand.

AT: https://www.desmos.com/calculator/mlbvj3lg0f

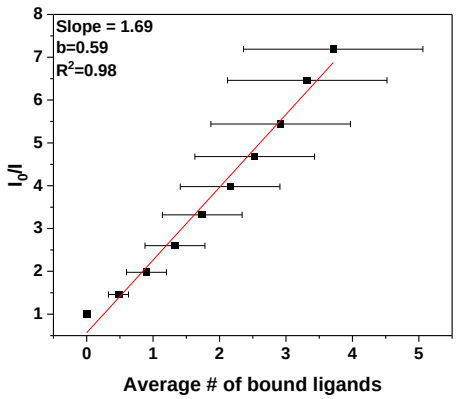

Figure Sd. SV experiment with AT ligand.

ADT: https://www.desmos.com/calculator/hlw5khl7zl

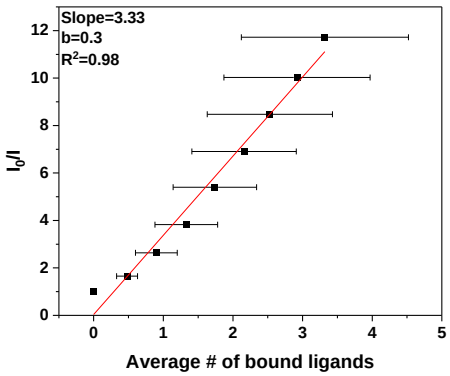

Figure Se. SV experiment with ADT ligand.

Although the linear fit lies within the experimental error bars and is thus not strictly excluded by the data, it performs poorly for strong quenchers and fails to capture the expected initial condition at (0,1). In contrast, the Poisson-based model provides significantly better agreement across the full range of data, especially with strong quenchers such as AT and ADT. Notably, in the limit of weak quenchers, the Poisson model converges to a linear dependence, resulting in similar outcomes for both models. However, for strong quenchers, deviations from linearity are pronounced, particularly at low x values, and the Poisson model becomes essential for accurately describing the quenching behavior.

-All experiments were done in a 1cm cuvette and were performed at room temperature (25°C). To determine the average number of ligands (*x*) we used the equation:

$$x = \frac{A_X \varepsilon_{QD}}{A_{QD} \varepsilon_X}$$

Where x is the average number of ligands, A_X is the absorption of ligand X, ε_X is the molar absorptivity of ligand X, A_{QD} is the absorption of QD and ε_{QD} is the molar absorptivity of QD.

And therefore, the error in x is:

$$\left(\frac{\Delta x}{x}\right)^2 = \left(\frac{\Delta A_{QD}}{A_{QD}}\right)^2 + \left(\frac{\Delta \varepsilon_{QD}}{\varepsilon_{QD}}\right)^2 + \left(\frac{\Delta A_X}{A_X}\right)^2 + \left(\frac{\Delta \varepsilon_X}{\Delta \varepsilon_X}\right)^2$$

Because the uncertainties in the extinction coefficients are much larger than the error in the absorbance measured by the spectrophotometer, the latter can be neglected.

$$\left(\frac{\Delta x}{x}\right)^2 = \left(\frac{\Delta \varepsilon_{QD}}{\varepsilon_{QD}}\right)^2 + \left(\frac{\Delta \varepsilon_X}{\varepsilon_X}\right)^2$$

The uncertainties in the extinction coefficients were taken to be around 500$M^{-1}cm^{-1}$. The error originates from the measurement of the extinction

coefficients of the ligands. The same error was assigned to the QD extinction coefficient, even though we did not measure it ourselves and the value was taken from the literature[5].

- All Stern–Volmer (SV) experiments were performed approximately 2–3 times to verify reproducibility. Although the presented data are from single representative measurements, the repeated experiments showed consistent trends and comparable results.
- In the experiment with PT, no absorption of the ligand can be observed, therefore we assumed that all the PT molecules we are add replace the OA ligands. It is a reasonable assumption since thiol groups are more strongly bound to the Cd ions.
- $\frac{I_0}{I(x)}$ calculated by measuring the emission spectrum of the QD with and without a quencher and calculating the area under the emission graph of the QD with and without a quencher. And finally to take the ratio of the areas without quencher and with.
- Additionally, we assumed that all TP molecules bind to the QDs, as thiol groups are known to have a much stronger binding affinity to Cd compared to carboxylic acid groups. Furthermore, the photochemical stability of the AT and ADT QD system was low under light exposure, causing decomposition of both the ligands and QDs (Figures S18 and S19). In the absence of oxygen, only the ligands decomposed, while in the presence of oxygen, the QDs also decomposed, likely due to singlet oxygen formation sensitized by the ligands. However, the process is relatively slow and does not affect the results on the timescale of the measurements performed.
- Simplification the sum:

$$A = \sum_{n=1}^{\infty} \frac{x^n}{n!} e^{-x} \frac{1}{b+n} = \sum_{n=1}^{\infty} \frac{x^n}{n!} e^{-x} \int_0^1 t^{b+n-1} dt = \int_0^1 e^{-x} t^{b-1} \sum_{n=1}^{\infty} \frac{t^n x^n}{n!} dt$$
$$= \int_0^1 e^{-x} t^{b-1} \sum_{n=1}^{\infty} \frac{t^n x^n}{n!} dt = \int_0^1 e^{-x} t^{b-1} e^{tx} dt = \int_0^1 e^{x(t-1)} t^{b-1} dt$$

The integral for b=1 is equal to:

$$A = \frac{1}{x} - \frac{e^{-x}}{x}$$

and therefore: $\frac{I_0}{I(x)} = \frac{1}{\frac{1}{x} - \frac{e^{-x}}{x}}$ and when x is large: $\frac{I_0}{I(x)} = \frac{1}{\frac{1}{x} - \frac{e^{-x}}{x}} = x$

The integral for b>>1:

First we will change variable $u = 1 - t$:

$$\int_0^1 e^{x(t-1)} t^{b-1} dt = \int_1^0 (1-u)^{b-1} e^{-xu} (-du) = \int_0^1 (1-u)^{b-1} e^{-xu} du$$

When b>>1 or m>>1 $(1-u)^{b-1} e^{-xu}$ has significant values only around 0. So we can approximate the function:

$$(1-u)^{b-1} e^{-xu} = e^{-u(b-1)} e^{-xu} = e^{-u(b+x-1)}$$

And the integral is now:

$\int_0^1 e^{-u(b+x-1)}du$

When b>>1 or m>>1 Contributions to integration after 1 are negligible (since the function decays exponentially), so we can change the limit of the integral to ∞.

$$\int_0^\infty e^{-u(b+x-1)}du = \frac{1}{b+x-1} \rightarrow \frac{I_0}{I(x)} = \frac{b^{-1}}{\frac{1}{b+x-1}} = 1 + \frac{x}{b} - \frac{1}{b}$$

When b>>1 or m>>1 this equal to: $\frac{I_0}{I(x)} = 1 + \frac{x}{b}$

For $b \rightarrow 0$:

We will start with equation 3:

$$\frac{I_0}{I(x)} = \frac{b^{-1}}{\sum_{n=1}^{\infty}\frac{x^n}{n!}e^{-x}\frac{1}{b+n}} = \frac{b^{-1}}{e^{-x}\frac{1}{b} + xe^{-x}\frac{1}{b+1} + \frac{x^2}{2}e^{-x}\frac{1}{b+2} + \cdots} = \frac{b^{-1}}{e^{-x}b^{-1}(1 + x\frac{1}{1+\frac{1}{b}} + \frac{x^2}{2}\frac{1}{1+\frac{2}{b}} + \frac{x^3}{6}\frac{1}{1+\frac{3}{b}} + \cdots)}$$

The terms $x\frac{1}{1+\frac{1}{b}}$, $\frac{x^2}{2}\frac{1}{1+\frac{2}{b}}$, $\frac{x^3}{6}\frac{1}{1+\frac{3}{b}}$, ... are equal to zero in the limit of $b \rightarrow 0$

$$\frac{b^{-1}}{e^{-x}b^{-1}(1 + x\frac{1}{1+\frac{1}{b}} + \frac{x^2}{2}\frac{1}{1+\frac{2}{b}} + \frac{x^3}{6}\frac{1}{1+\frac{3}{b}} + \cdots)} = e^x \rightarrow \frac{I_0}{I(x)} = e^x$$

- Estimate the energy transfer efficiencies between the QDs and three ligands: From the SV experimental results, it is also possible to determine the TET efficiency, If we assume that the quenching resulting from the bound molecule is solely due to TET, the following equation can be used: $\phi_{TET}(x) = 1 - \frac{I(x)}{I_0} = 1 - \frac{\sum_{n=1}^{\infty}\frac{x^n}{n!}e^{-x}\frac{1}{b+n}}{b^{-1}}$.

  Derivation:

  the definition of TET efficiency is:

  $$\phi_{TET} = \frac{k_{TET}}{k_r + k_{nr} + k_{TET}}$$

  $$\phi_{TET} = \frac{k_{TET}}{k_r + k_{nr} + k_{TET}} = \frac{k_{TET} + k_r + k_{nr} - (k_r + k_{nr})}{k_r + k_{nr} + k_{TET}} = \frac{k_{TET} + k_r + k_{nr}}{k_r + k_{nr} + k_{TET}} - \frac{k_r + k_{nr}}{k_r + k_{nr} + k_{TET}} = 1 - \frac{\tau_q}{\tau_0}$$

  $$= 1 - \frac{I(x)}{I_0}$$

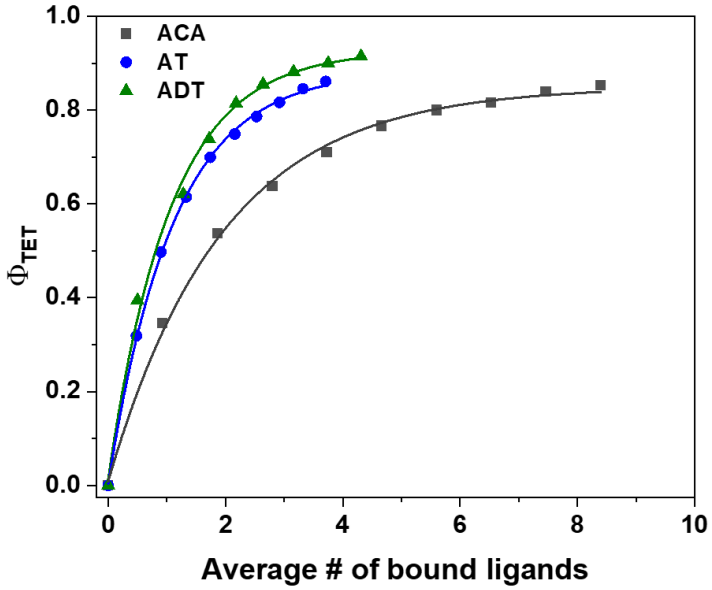

Figure Se. TET efficiency as a function of ligand coverage for ACA, AT and ADT.

Name	b	k_q(ns^{-1})
TP	20.9 ± 0.5	0.00399 ± 0.0001
ACA	1.23 ± 0.1	0.068 ± 0.006
AT	0.37 ± 0.2	0.2 ± 0.1
ADT	0.24 ± 0.1	0.3 ± 0.1

Table S2. b and k_q values for the different ligands.

General graphs

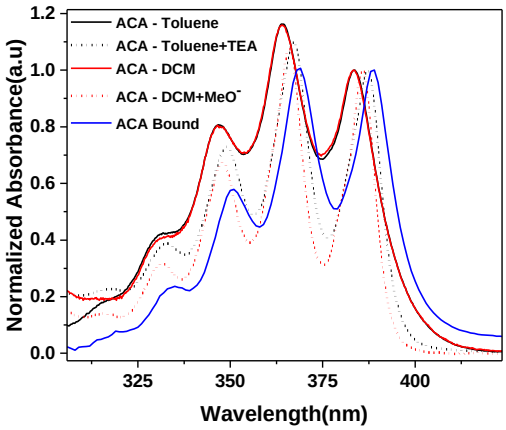

Figure S3. Absorption spectra of ACA in toluene (black), in toluene and trimethylamine (dotted black), in DCM (red), in DCM and methoxide (dotted red), and bound to CdSe–OA(blue).

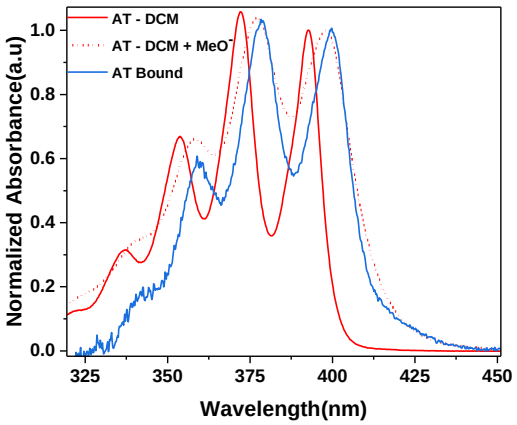

Figure S4. Absorption spectra of AT in DCM (red), in DCM and methoxide (dotted red), and bound to CdSe–OA (blue).

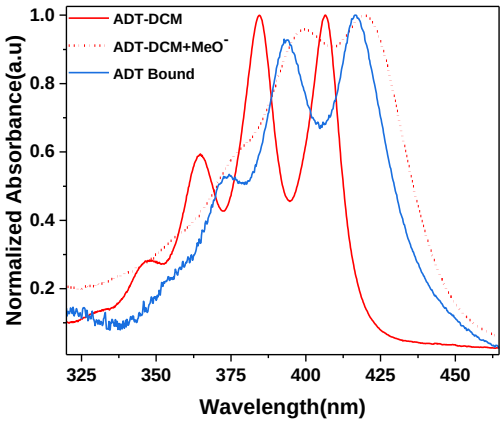

Figure S5. Absorption spectra of ADT in DCM (red), in DCM and methoxide (dotted red), and bound to CdSe–OA (blue).

In all three ligands, the intensity of the 0-0 transition is higher relative to other vibronic transitions compared to their deprotonated forms. This suggests that the geometry of the ground and excited states is more similar in the bound (protonated) forms than in the deprotonated ones. A possible explanation is the crowded environment of the OA ligands on the QD surface. Moreover, the energy transitions are generally similar between the bound and deprotonated forms, with minor differences that may result from electronic coupling. Overall, deprotonation is the main factor responsible for the changes observed upon binding.

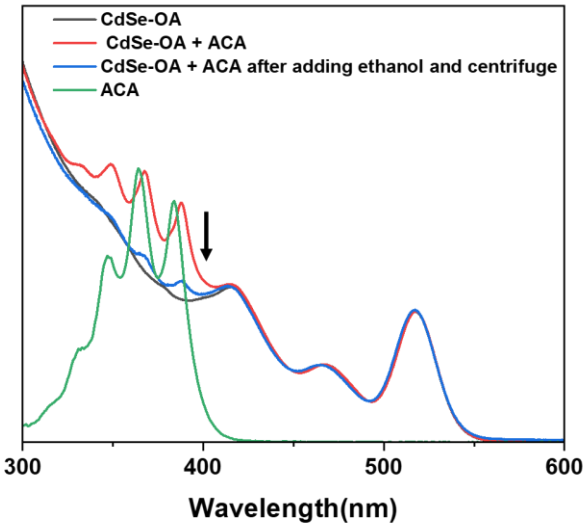

Figure S6. Absorption spectrum of CdSe-OA (black), CdSe-OA with ACA add (red) and one washing cycle Adding ethanol in the cleaning process causes bound ACA to detach (blue). This is after one cycle, usually in previous works 3 cycle of cleaning are done.

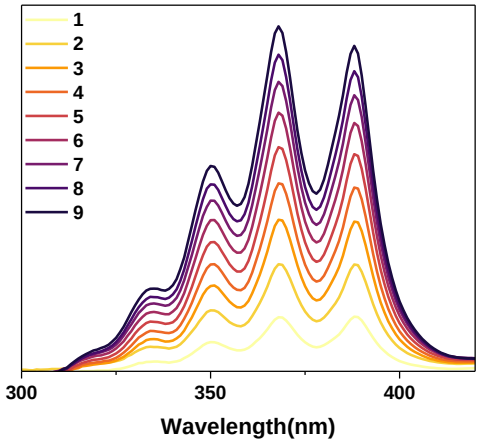

Figure S7. Absorption spectrum of bound ACA ligand in toluene solvent as a function of average coverage of ACA molecules in CdSe-OA solution. The spectrum of the ligand is made by subtracting the spectrum of the QD from the original spectrum of the ACA and the QD.

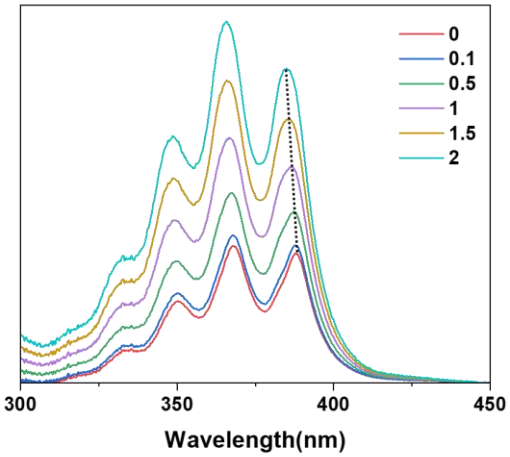

Figure S8. Linear combination of normalized absorption spectrum of bound and free ACA. the numbers are the ratio of $\frac{ACA_F}{ACA_B}$, where F means free and B means bound. It can be seen that the ratio increases, the spectrum undergoes distortion and the peaks shift to the blue region.

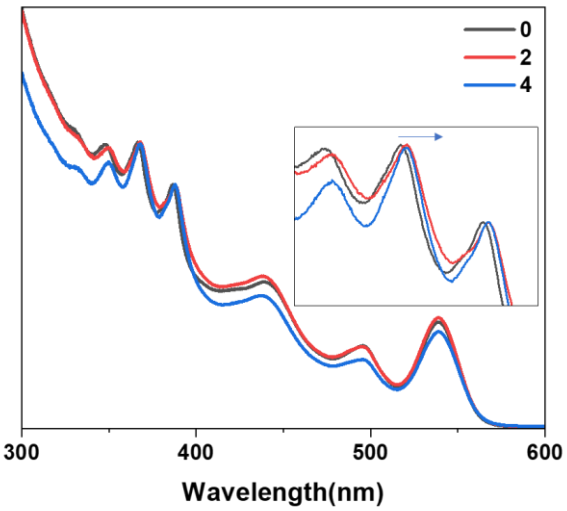

Figure S9. Absorption spectrum of CdSe-OA with no pre-washing(black), with 2 pre-washing(red) and with 4 pre-washing(blue). Before ligand adding, washing with a solvent (hexane) followed by an anti-solvent (methanol) lead to detachment of ligands and creates empty sites in QDs. It can be seen that pre-washing causes a shift in the absorption of the ligands. After 4 washes there is no further change in the absorption spectrum. This supports that if there are free OA ligands there is less binding of ACA (Figure S2).

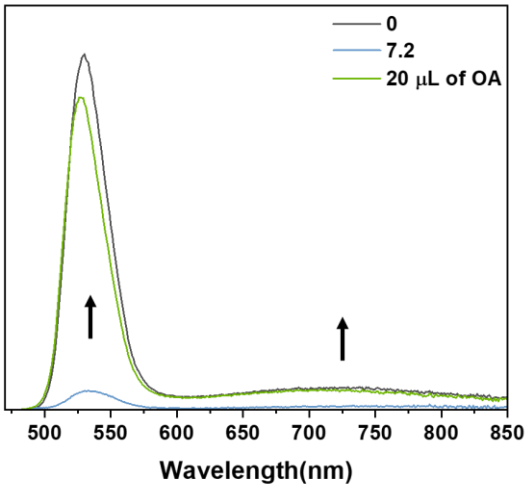

Figure S10. PL spectra of OA-CdSe QDs before adding ACA(black), after adding ACA such that the average number of bound ligands is 7.2 (blue) and after adding 20 microliter of OA ligand (green).

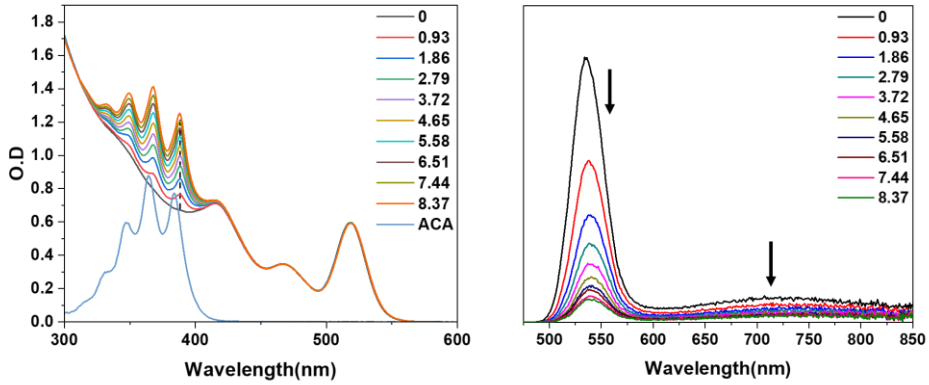

Figure S11. Abs (right) and PL (left) specters for SV experiment of ACA.

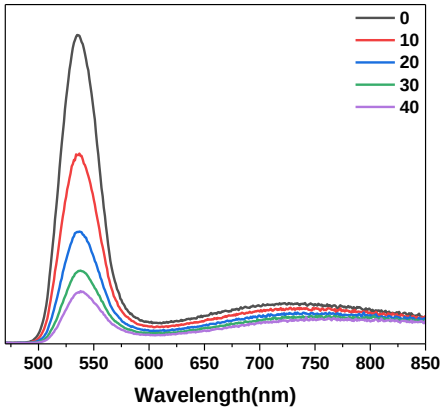

Figure S12. PL spectra for SV experiment of PT.

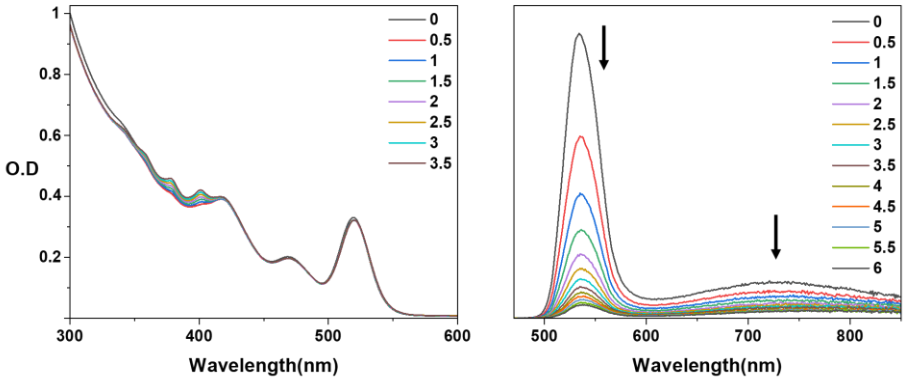

Figure S13. Abs (right) and PL (left) specters for SV experiment of AT.

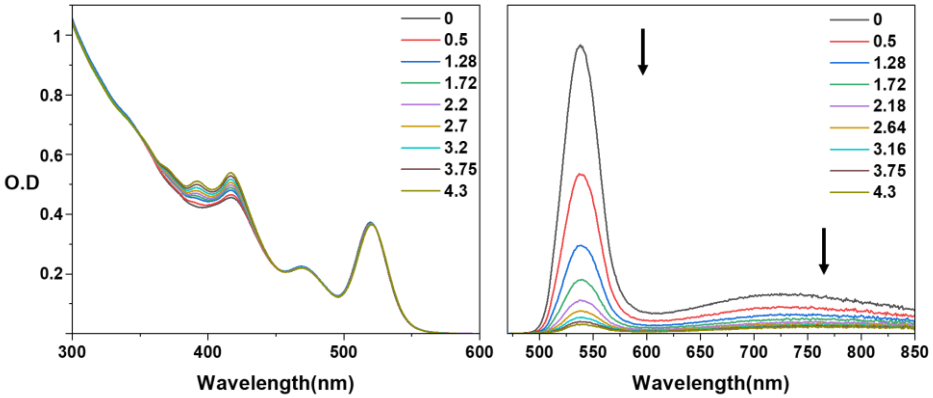

Figure S14. Abs (right) and PL (left) specters for SV experiment of ADT.

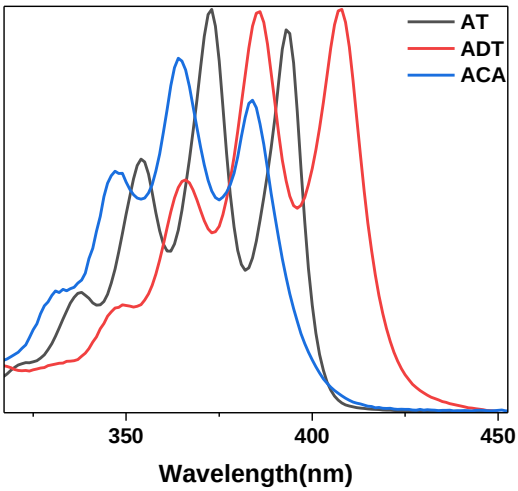

Figure S15. Abs spectra in toluene of ACA, AT and ADT ligands.

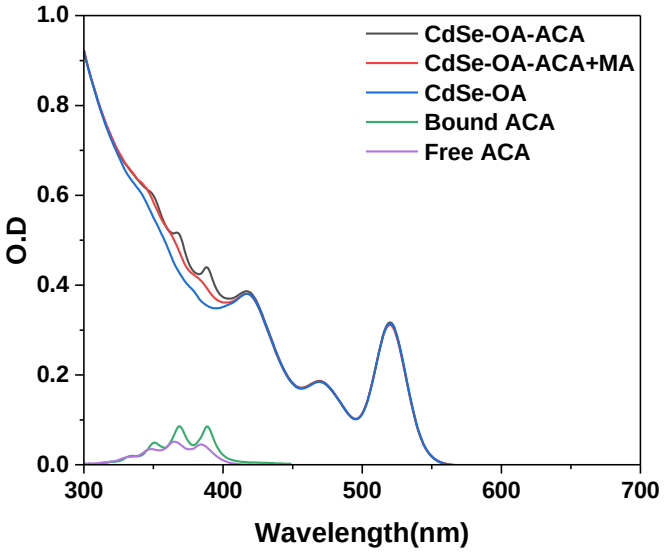

Figure S16. Absorption spectra in toluene of CdSe-OA, CdSe-OA-ACA, and CdSe-OA-ACA+MA (myristic acid). Upon adding MA to the CdSe-OA-ACA solution, a change in the spectrum is observed. To determine if this change is due to the absorbance of the ACA ligand, we subtracted the CdSe-OA spectrum from the CdSe-OA-ACA spectrum. The resulting difference reveals the absorption spectra of the bound and free ACA. meaning MA exchange with ACA.

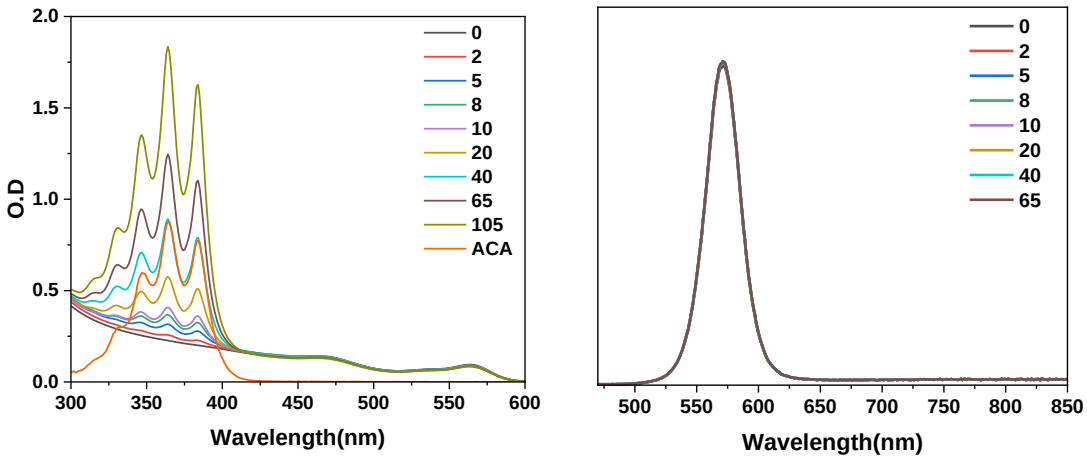

Figure S17. Left: Absorption spectrum in toluene solvent as a function of the ACA to CdSe-TOP/TOPO/ODPA ratio, no shift is observed. Right: CdSe-TOP/TOPO/ODPA photoluminescence as a function of the ACA to CdSe-TOP/TOPO/ODPA ratio in toluene solvent, with excitation at 450 nm.

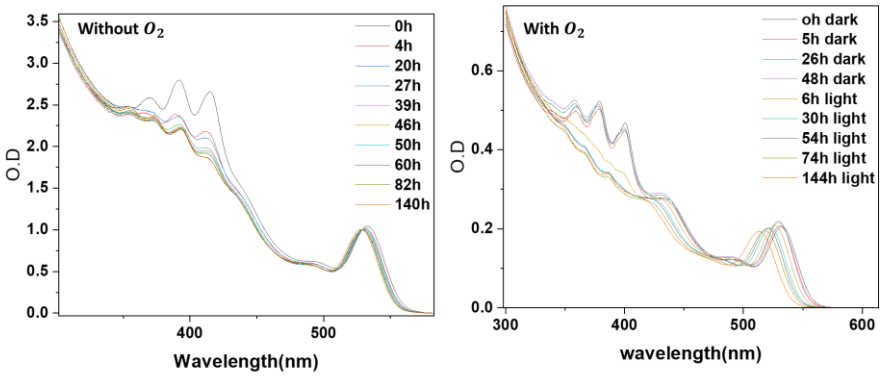

Figure S18. Absorption spectra in toluene of CdSe-OA-ADT under two conditions: with oxygen (right) and without oxygen and with light (left). In the presence of light, a photochemical reaction is observed over time, causing changes in the ligands. In contrast, when no light is applied, the system remains stable. Additionally, in the presence of light and oxygen, a change in the QDs is observed: the QDs size decrease, as evidenced by the blue shift in the band edge absorption.

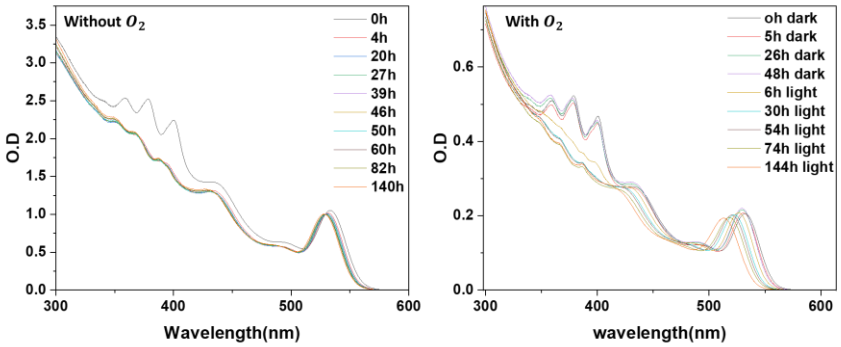

Figure S19. Absorption spectra in toluene of CdSe-OA-AT under two conditions: with oxygen (right) and without oxygen and with light (left). In the presence of light, a photochemical reaction is observed over time, causing changes in the ligands. In contrast, when no light is applied, the system remains stable. Additionally, in the presence of light and oxygen, a change in the QDs is observed: the QDs size decrease, as evidenced by the blue shift in the band edge absorption.

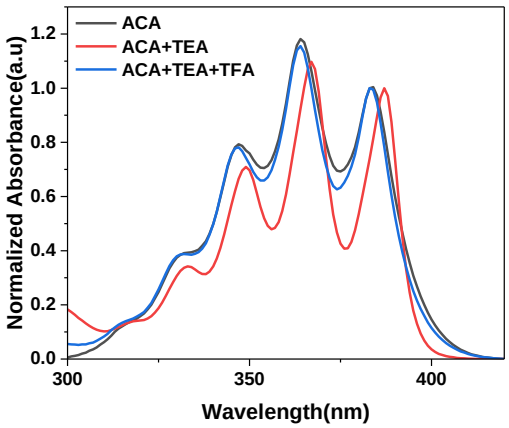

Figure S20. Absorption spectra in toluene of ACA (black), ACA with trimethylamine (TEA) add (red, deprotonated form of ACA), deprotonated ACA with Trifluoroacetic acid (TFA) add (blue, protonated form of ACA).

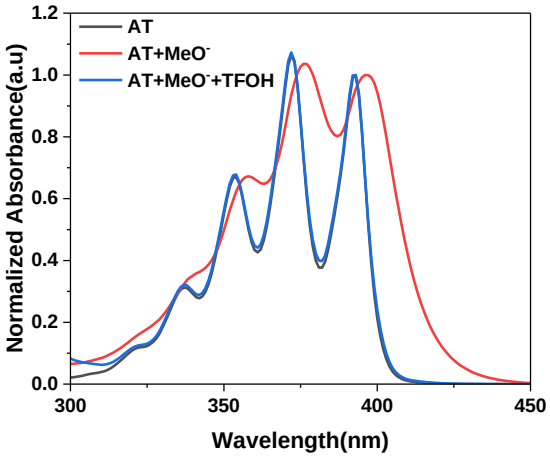

Figure S21. Absorption spectra in DCM (dichloromethane) of AT (black), AT with Methoxide (MeO^-) add (red, deprotonated form of AT), deprotonated AT with Trifluoromethanesulfonic acid (TFOH) add (blue, protonated form of AT).

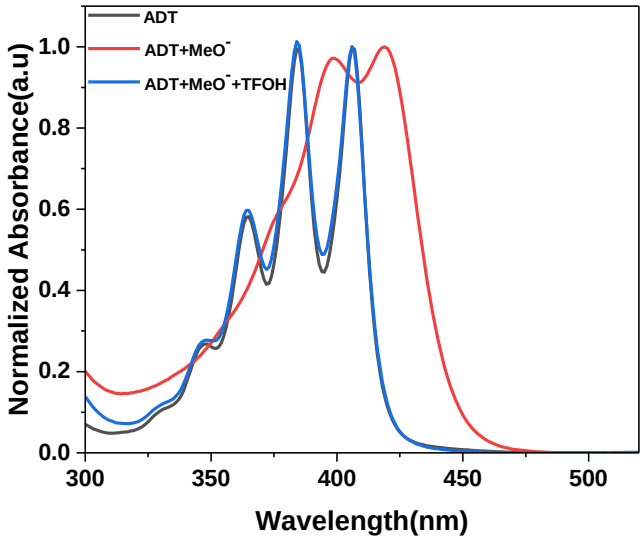

Figure S22. Absorption spectra in DCM (dichloromethane) of ADT (black), ADT with Methoxide (MeO^-) add (red, deprotonated form of ADT), deprotonated ADT with Trifluoromethanesulfonic acid (TFOH) add (blue, protonated form of ADT).

Upconversion Experiments

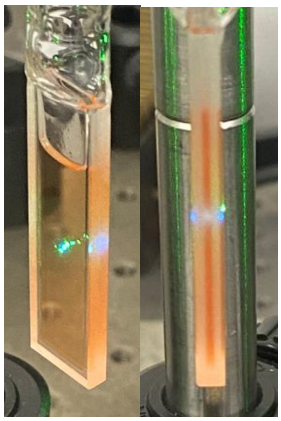

Figure S23. A solution of CdSe-QD with AT and DPA (9,10-diphenylantracene) irradiated with a 532 nm laser, resulting in clearly observable blue emission. This observation shows that the thiolated ligands, in combination with the QDs, indeed facilitate triplet energy transfer.

Calculations

Calculations were carried out with the Gaussian 16[7] series of programs using density function theory (DFT). The functional we have chosen is CAM-B3LYP with basis set of cc-pVTZ. No symmetry restrictions were applied in any of the optimal geometries presented. The optimal geometries for all structures were confirmed as minima by frequency calculations. No negative frequencies were found for any stationary points presented in this work.

Name	HOMO(eV)	LUMO(eV)
ACA	**-6.972**	**-1.103**
AT	**-6.765**	**-0.933**
ADT	**-6.771**	**-1.088**

Table S3. Calculated HOMO and LUMO of the ligands

References

[1] E. M. Mathew, T. Devassia, S. Prathapan, P. A. Unnikrishnan, *ARKIVOC* **2018**, *2019*, 10–18.

[2] M. W. Miller, R. W. Amidon, P. O. Tawney, *J. Am. Chem. Soc.* **1955**, *77*, 2845–2848.

[3] J. Zhou, M. Zhu, R. Meng, H. Qin, X. Peng, *J. Am. Chem. Soc.* **2017**, *139*, 16556–16567.

[4] O. Chen, J. Zhao, V. P. Chauhan, J. Cui, C. Wong, D. K. Harris, H. Wei, H.-S. Han, D. Fukumura, R. K. Jain, M. G. Bawendi, *Nat. Mater.* **2013**, *12*, 445–451.

[5] K. Gong, J. E. Martin, L. E. Shea-Rohwer, P. Lu, D. F. Kelley, *J. Phys. Chem. C* **2015**, *119*, 2231–2238.

[6] O. Elimelech, O. Aviv, M. Oded, X. Peng, D. Harries, U. Banin, *ACS Nano* **2022**, *16*, 4308–4321.

[7] M. J. Frisch, G. W. Trucks, H. B. Schlegel, G. E. Scuseria, M. A. Robb, J. R. Cheeseman, G. Scalmani, V. Barone, G. A. Petersson, H. Nakatsuji, X. Li, M. Caricato, A. V. Marenich, J. Bloino, B. G. Janesko, R. Gomperts, B. Mennucci, H. P. Hratchian, J. V. Ortiz, A. F. Izmaylov, J. L. Sonnenberg, R. F. Williams, F. Ding, F. Lipparini, F. Egidi, J. Goings, B. Peng, A. Petrone, T. Henderson, D. Ranasinghe, V. G. Zakrzewski, J. Gao, N. Rega, G. Zheng, W. Liang, M. Hada, M. Ehara, K. Toyota, R. Fukuda, J. Hasegawa, M. Ishida, T. Nakajima, Y. Honda, O. Kitao, H. Nakai, T. Vreven, K. Throssell, J. A. Montgomery Jr., J. E. Peralta, F. Ogliaro, M. J. Bearpark, J. J. Heyd, E. N. Brothers, K. N. Kudin, V. N. Staroverov, T. A. Keith, R. Kobayashi, J. Normand, K. Raghavachari, A. P. Rendell, J. C. Burant, S. S. Iyengar, J. Tomasi, M. Cossi, J. M. Millam, M. Klene, C. Adamo, R. Cammi, J. W. Ochterski, R. L. Martin, K. Morokuma, O. Farkas, J. B. Foresman, D. J. Fox, **2016**.